COMMUNICATION

Intracellular Distribution of Macrophage Targeting Ferritin–Iron Oxide Nanocomposite

By *Masaki Uchida, Deborah A. Willits, Karin Muller, Ann F. Willis, Larissa Jackiw, Mark Jutila, Mark J. Young, Alexandra E. Porter,** and *Trevor Douglas**

Nanoparticles exhibit unique size-dependent properties and are able to pass biological barriers that are normally inaccessible to larger particles, such as blood–brain barrier and blood vessel pores.[1–3] Therefore, they have the possibility of being developed into new diagnostic and therapeutic tools. More recently, the development of nanoparticles with multifunctionality, such as cell/tissue-specific delivery, disease imaging, and therapy, has drawn the interest of material and medical scientists.[4–9] Various types of materials, such as polymers and lipids, have been increasingly utilized as platforms for nanoparticles.[10] Among them, biomimetic approaches exploiting protein-cage architectures, such as viral capsids and ferritin, have unique advantages over other materials.[11,12] Protein cages are self-assembled architectures composed of well-defined numbers of subunits. Their structure and size are precisely controlled at the atomic level, since they are gene products. They also possess distinct interfaces (e.g., inside and outside), which can be modified either genetically and/or chemically to impart multifunctionality for targeted delivery of imaging and therapeutic agents.[11,13,14] The preciseness of the protein-cage architectures allows us to introduce modifications at well-defined positions by design. For example, a cell-specific targeting peptide can be introduced on a unique position on the exterior surface, while the interior can sequester (and protect) an imaging or therapeutic agent.[8] While these materials hold significant promise for nanomedicine, it is critical to investigate the observed targeting in more detail, at a single-cell level, to understand both the efficiency and potential toxicity of a protein-cage-based material.

We have developed a human ferritin (HFn)–iron oxide nanocomposite to act as magnetic resonance imaging (MRI) contrast agent, in order to image macrophages that are involved in inflammatory diseases, such as atherosclerosis.[15] It has been confirmed that the protein–mineral composite is taken up by macrophages at levels comparable to commercially available contrast agents, ferumoxides, and have the potential to act as MRI contrast agents to assess the state of macrophage-rich atherosclerotic plaques.[15] Furthermore, we have genetically engineered a ferritin mutant displaying 24 copies of an RGD-4C peptide,[7] which binds selectively to integrin $\alpha_v\beta_3$ and integrin $\alpha_v\beta_5$[16,17] on the exterior surface of the protein cage. Integrin $\alpha_v\beta_3$ is known to play an important role in the initiation or progression of some human diseases such as rheumatoid arthritis and cancer.[18,19] Even in the case of atherosclerosis, it has been reported that integrin $\alpha_v\beta_3$ is readily detected on macrophages in early and advanced human atherosclerotic lesions, where its expression is upregulated by stimuli of oxidized low-density lipoprotein, one of the key components in the progression of the disease.[19] Therefore, it is expected that the ferritin variant, conjugated with the RGD-4C targeting peptide (RGD4C-Fn), will target macrophages and accomplish detection of inflammatory diseases at early stages. However, it is unclear if the particles, which bind to cell surface exposed integrins, can be internalized within the cell. The intracellular distribution of such cell-targeting nanoparticles in comparison with nontargeting particles has not been well addressed. Direct observation of the particles inside cells will provide valuable information to understand the interaction and intracellular fate of these particles. The aims of this work were to i) evaluate the macrophage-cell-targeting ability of RGD4C-Fn in vitro and (ii) assess the intracellular distribution of targeted (RGD4C-Fn) and nontargeted (HFn) iron oxide composite particles in macrophage cells.

The relative targeting abilities of RGD4C-Fn and HFn toward macrophages were first evaluated using fluorescence-activated cell sorting (FACS) and epifluorescence microscopy. HFn and RGD4C-Fn were heterologously expressed, as previously described, and conjugated with fluorescein-5-maleimide.[7]

[*] Dr. A. E. Porter
Department of Materials, Imperial College London
London SW7 2AZ (UK)
SuperSTEM, Daresbury Laboratory
Cheshire WA4 4AD (UK)
E-mail: a.porter@imperial.ac.uk
Prof. T. Douglas, Dr. M. Uchida, A. F. Willis
Department of Chemistry and Biochemistry
and the Center for Bio-Inspired Nanomaterials
Montana State University, Bozeman, MT 59717 (USA)
E-mail: tdouglas@chemistry.montana.edu
D. A. Willits, Prof. M. J. Young
Department of Plant Sciences
and the Center for Bio-Inspired Nanomaterials
Montana State University, Bozeman, MT 59717 (USA)
Dr. K. Muller
Department of Physiology, Development and Neuroscience
Multiimaging Centre
University of Cambridge, Anatomy Building
Cambridge CB2 3DY (UK)
L. Jackiw, Prof. M. Jutila
Department of Veterinary Molecular Biology
Montana State University
Bozeman, MT 59717 (USA)

DOI: 10.1002/adma.200801209

According to transmission electron microscopy (TEM), both HFn and RGD4C-Fn present a cage-like structure with approximately 12 nm in diameter, and those two cages were indistinguishable in their size and morphology (Fig. S1 of Supporting Information).

FACS was used to quantify the ability of fluorescently labeled protein cages to bind THP-1 human acute monocytic-leukemia cells.[20,21] THP-1 cells incubated with fluorescently labeled RGD4C-Fn exhibit a geometric (geo.) mean fluorescence intensity value of 198 (Fig. 1). This value is much higher than the autofluorescence of the cells (geo. mean fluorescence intensity value of 4), and comparable to the positive control experiment (geo. mean value of 181), in which THP-1 cells were incubated with a fluorescein-conjugated anti-integrin $\alpha_v\beta_3$ antibody. Although the cells incubated with nontargeting HFn showed nonspecific binding with the cage (geo. mean value of 39), this is significantly smaller (five-fold less) than the cells incubated with RGD4C-Fn. These data clearly suggest that RGD4C-Fn exhibit enhanced interaction with THP-1 cells compared to nontargeting HFn.

THP-1 cells incubated with fluorescently labeled cages were imaged by epifluorescence microscopy to visualize fluorescently labeled protein cages bound to THP-1 cells. For direct comparison of epifluorescence data, the concentration of fluorescein, the illumination intensity, and the camera exposure time were held constant. RGD4C-Fn was observed to bind to THP-1 cell as well as to fluorescein-conjugated anti-integrin $\alpha_v\beta_3$ antibody (Fig. S2 of Supporting Information). This is consistent with the FACS analysis result, indicating that fluorescently labeled HFn binds to the cell but to a much lower degree than RGD4C-Fn. It has been demonstrated that the RGD4C-Fn does not exhibit specific binding to noncancerous T-cells, which do not express integrin $\alpha_v\beta_3$.[7] In combination with previous studies, the present data indicate that RGD4C-Fn exhibits selective targeting toward macrophage cells, mediated by binding to integrin $\alpha_v\beta_3$.

The iron oxide mineralization reaction to form encapsulated and constrained Fe_3O_4 nanoparticles within the cages was previously described, and the size distribution of mineral cores ((5.1 ± 0.9) and (5.4 ± 0.9) nm for the HFn and RGD4C-Fn, respectively) showed no significant difference between HFn and RGD4C-Fn nanoparticles (Fig. S3 of Supporting Information). A decrease of up to 8% of cell viability was observed when the cells were incubated with 1 or 2 μg mL^{-1} of the mineralized HFn or RGD4C-Fn, compared to the cell-only control. However, there was no statistically significant difference in toxicity between the particles ($p < 0.01$) (Fig. S4 of Supporting Information). Since both the mineralized protein cages and neutral red dye are accumulated into lysosomes, accumulation of dye may be altered by the mineralized protein cages at high concentrations, leading to artificially lowered viability determinations. Since toxicity assessment of the mineralized protein cages is critical for proceeding to clinical studies, further in vitro and in vivo investigations are required.

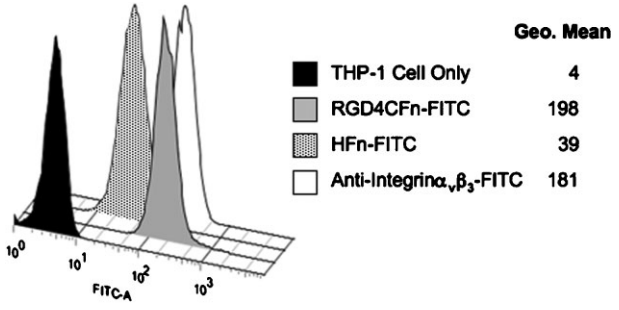

Figure 1. FACS analysis of THP-1 monocyte cells incubated with fluorescently labeled protein cages. The data are plotted as histograms with their corresponding geometric (geo.) mean fluorescence values. Although the nontargeted protein cage (HFn) showed some interaction with the cells, the targeted cages (RGD4C-Fn) exhibit significantly increased interaction with the cells.

To evaluate the internalization and intracellular distribution of the targeted and nontargeted protein-cage nanoparticles, we have utilized scanning transmission electron microscopy (STEM) with a high-angle annular dark field (HAADF) detector and energy filtered transmission electron microscopy (EFTEM) techniques to directly image the intracellular particle location. Previous work has highlighted the development of these techniques for intracellular evaluation of C_{60}[22,23] and single-walled carbon nanotubes[24] taken up by monocyte-derived macrophage cells. HAADF-STEM collects electrons that undergo Rutherford scattering. HAADF-STEM images can be acquired where the intensity is approximately proportional to Z^2 (Z is the atomic number of the scattering atom). For this reason, this technique is extremely sensitive to atomic number, and is ideal for imaging iron inside the Fn cage, to establish the subcellular distribution of the iron oxide mineralized HFn (nontargeting) and RGD4C-Fn (targeting) particles.

The distribution of iron oxide nanoparticles within the cell was investigated within both stained and unstained sections, because there is a possibility of staining artifacts, which could cause misidentification of the iron nanoparticles, while metal-staining techniques lead to high contrast. HAADF-STEM observation of both stained and unstained sections of macrophage cells incubated with the mineralized RGD4C-Fn revealed bright clusters, consistent with iron oxide nanoparticles, encapsulated within the protein cages. These were observed mainly within lysosomes and cytoplasm (Fig. 2). Even though the bright particles were observed within cells incubated with the mineralized HFn (Fig. 3), there were significantly fewer particles in the cells incubated with the HFn than in those incubated with RGD4C-Fn. It is well known that nanoparticles are cleared by the mononuclear phagocyte system by phagocytosis and/or pinocytosis.[25] In previous in vitro[26] and in vivo[27] studies, it has been confirmed that ultrasmall superparamagnetic iron oxide (USPIO) nanoparticles are accumulated in lysosomes/phagosomes of macrophages. Accumulation of the HFn and RGD4C-Fn in the lysosomal compartment is therefore consistent with the literature. Accumulation of RGD4C-Fn in lysosomes is much more pronounced than for HFn. Integrins are capable of mediating phagocytosis,[28] and integrin $\alpha_v\beta_3$ and integrin $\alpha_v\beta_5$ in particular have been reported to be involved in the clearance of apoptotic cells.[29,30] This integrin-dependent phagocytosis pathway could be the reason for the more effective internalization of RGD4C-Fn into macrophages. This implies that conjugation of the RGD-4C peptide with the protein cage could be advantageous not only for targeting macrophages but also for enhancing internalization of the particles into the cells. It should be noted that in some TEM sections the iron oxide particles were found

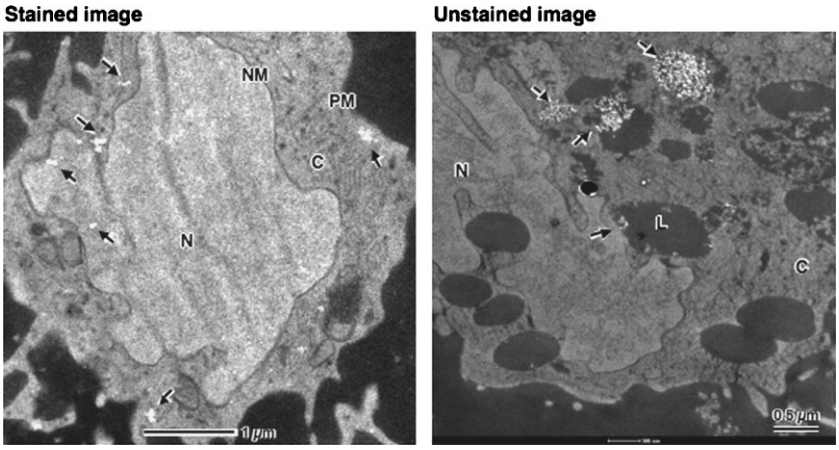

Figure 2. Stained (left) and unstained (right) HAADF-STEM images of monocyte-derived macrophage cells incubated with RGD4CFn-Fe. (C: the cytoplasm, L: the lysosome, N: the nucleus, NM: the nuclear membrane, and PM: the plasma membrane). Bright particles indicated by arrows are the mineralized RGD4C-Fn.

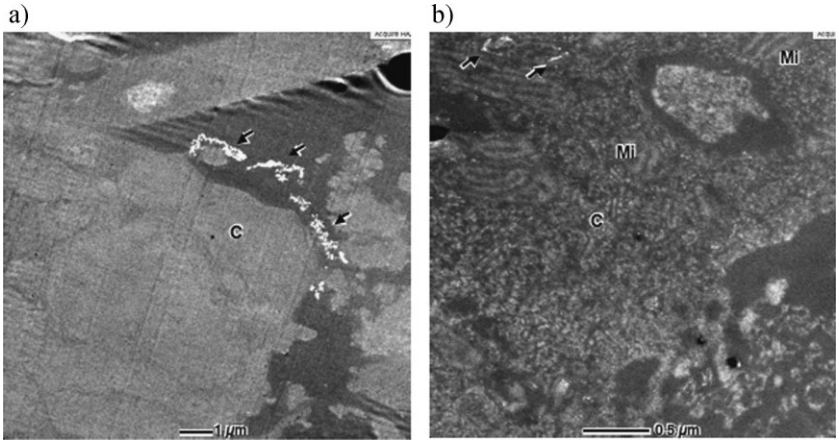

Figure 3. HAADF-STEM image of unstained monocyte-derived macrophage cells incubated with HFn-Fe, showing the cytoplasm (C), mitochondria (Mi), and the mineralized Fn (indicated by arrow). The mineralized Fn are a) outside the cell and b) within the cytoplasm.

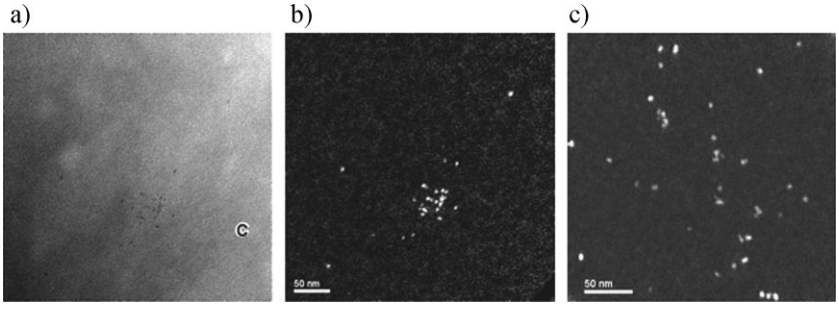

Figure 4. Unstained EFTEM images of macrophage cells incubated with iron oxide encapsulated HFn or RGD4C-Fn. a) Zero-loss bright-field image of a cell incubated with HFn. Light-gray region is the cytoplasm (C). Black dots within the cytoplasm are the mineralized HFn particles. b) Iron mapping captured from same area from image a). Bright spots contain iron. c) Iron mapping of a cell incubated with RGD4C-Fn. These images indicate that the mineralized HFn and RGD4C-Fn are accumulated within the cells.

within the nucleus of the cells incubated with RGD4C-Fn, while we found no evidence of the mineralized HFn within the nucleus. All unstained images in Figure 2 and 3 were obtained from sections 40 nm thin. Achieving contrast from cell organelles in unstained cell sections is challenging. Here we show that it is possible to achieve good contrast from cell organelles, such as the nucleus and mitochondria, without the need for stain, using ultrathin sections 40 nm thick and working in HAADF-STEM mode.

EFTEM techniques for imaging the particles were used to establish that the bright particles found within the cells were indeed iron oxide nanoparticles. ''Zero-loss'' mode is often used in EFTEM, because the contrast of bright-field TEM images is improved due to removal of inelastic scattered electrons. Alternatively, a map of a specific element can be acquired using characteristic absorption edges. Figure 4a and b show zero-loss and Fe maps captured from the same area of an unstained section of a macrophage cell incubated with the mineralized HFn. In Figure 4a, the light-gray region corresponds to the cytoplasm within the cell, and the black dots are electron-dense particles, due to inelastic scattering of electron beam. The Fe map clearly indicates the distribution of bright particles due to the iron, which correspond to the black particles in the zero-loss image. Together, these data indicate that the particles observed on the images are indeed the iron oxide particles from the mineralized HFn. A distribution of bright dots due to Fe was also observed within macrophage cells incubated with the mineralized RGD4C-Fn (Fig. 4c). It was clearly confirmed from these EFTEM images that both of the mineralized HFn and RGD4C-Fn are accumulated within the macrophage cells, suggesting an internalization of the nanoparticles.

Although there was some suggestion of the mineralized RGD4C-Fn located within the nucleus (Fig. 2), it was difficult to determine whether the particles were really inside the nucleus or were an artifact from sample preparation. Since translocated fragments of the mineralized particles that have broken up during sectioning would be found predominantly on the surface of sections, electron tomography obtained from thick section is feasible to confirm if the mineralized particles are within the nucleus. Figure 5 shows a series of horizontal slices through an HAADF-STEM reconstruction obtained from a thick (300 nm) section of a cell incubated with RGD4C-Fn. Some bright particles, believed to be the mineralized RGD4C-Fn

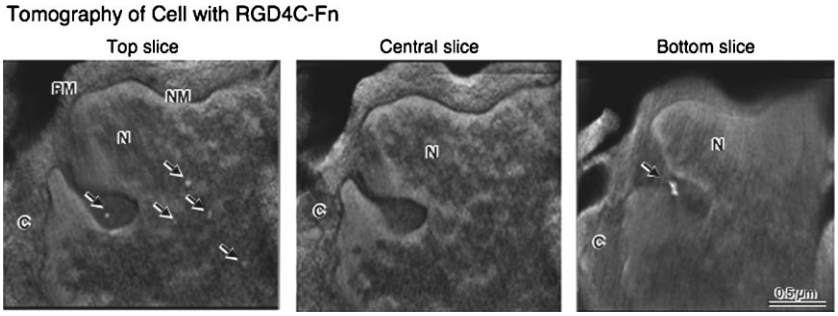

Figure 5. HAADF-STEM tomography of macrophage cell incubated with RGD4CFn-Fe. A series of horizontal slices through a HAADF-STEM reconstruction. (Arrows indicate the mineralized Fn, C: the cytoplasm, L: the lysosome, N: the nucleus, NM: the nuclear membrane, and PM: the plasma membrane). The height of top, central, and bottom slices are 25, 150, and 260 nm, respectively. The images suggest that some of the mineralized RGD4C-Fn particles are localized in the nucleus.

protein, were observed on the top slice image. These particles appear to be in the upper section of the nucleus. Because this is a section through the cell, it is unlikely that they are on the nucleus as a result of debris on the surface of the section, as they would then be out of this projection. The tomography therefore confirms that some of the RGD4C-Fn particles are able to traffic to the nucleus.

In summary, our data clearly indicate that RGD4C-Fn exhibits increased targeting capability toward macrophage cells, as compared to the control HFn. This is probably due to a specific binding of RGD-4C peptide to the cell surface exposed integrins $\alpha_v\beta_3$. This result holds the promise that RGD4C-Fn–iron oxide nanocomposites will have enhanced in vivo MR imaging capability toward macrophage-rich diseased tissue such as atherosclerotic plaques. According to the series of TEM observations, RGD4C-Fn protein-cage particles do not just bind to $\alpha_v\beta_3$ integrins on the cell surface, but are internalized into the cell much more effectively than HFn. Furthermore, the intracellular distribution of RGD4C-Fn and HFn seems to be different. In particular, RGD4C-Fn is found in the nucleus, whereas HFn is not. This may be simply because RGD4C-Fn has more opportunities to get into the nucleus due to a higher concentration of internalized particles, but there is also a possibility that the targeting particles have different internalization and migration pathways into the cell and further to the nucleus, as compared to nontargeted particles. This will be addressed in future work.

Experimental

Cloning of Human H Chain Ferritin and Genetic Engineering of RGD-4C Peptide Conjugated Ferritin (RGD4C-Fn): Human normal skeletal muscle cDNA was purchased from Invitrogen (D8090-01: Carlsbad, CA). The cloning, expression, and purification of RGD4C-Fn have been described elsewhere [7]. Briefly, the gene encoding the human H chain ferritin (HFn) was amplified by polymerase chain reaction (PCR) for amplification. The PCR product was subsequently cloned into NdeI/BamHI restriction enzyme sites of the pET-30a(+) plasmid (Novagen), for expression of the full-length proteins.

The N-terminus of the HFn was exposed toward the outside of the assembled ferritin cage. Therefore, if the targeting peptide, RGD-4C, was added at the N-terminus of the HFn subunit, it was expected that 24 copies of the peptide would be displayed on the exterior surface of HFn. In order to incorporate a gene sequence corresponding to the RGD-4C peptide onto the HFn plasmid, an AatII restriction site was introduced into the native HFn plasmid. The plasmid was digested by AatII and subsequently dephosphorylated by calf intestine alkaline phosphatase (CIP) enzyme. Complimentary primers 5′ GC GAC TGC CGC GGA GAC TGC ttc tgc GGA GGC GGA ACG T 3′ and 5′ TCC GCC TCC GCA GAA GCA GTC TCC GCG GCA GTC GCA CGT 3′ were mixed, annealed, and treated with kinase. The combined primers were ligated into the opened plasmid vector.

The plasmid of RGD4C-Fn was transformed into XL2 Blue ultracompetent *Escherichia coli* (Stratagene, La Jolla, CA, USA) and plated on LB with kanamycin plates for selection. Plasmid DNA was isolated from *E. coli*. The presence of HFn or RGD4C-Fn encoding genes was confirmed by sequencing the PCR-amplified product using an ABI 310 automated capillary sequencer using Big Dye chain-termination sequence technology (Applied Biosystem, Foster City, CA, USA).

Expression and Purification of RDG4C-Fn: RGD4C-Fn was expressed in *E. coli* [BL21 (DE3), Novagen] cultured in LB medium with kanamycin (30 mg L^{-1}). The protein production was induced by IPTG (1 mM) 4 h in advance of the cell harvest. The harvested cells were re-suspended in 45 mL of lysis buffer (100 mM HEPES, 50 mM NaCl, pH 8.0, 50 μg mL^{-1} of lysozyme, 60 μg mL^{-1} of DNase, 100 μg mL^{-1} of RNase). The suspension was incubated for 30 min at room temperature followed by cell disruption by a combination of French Press lysis and sonication on ice. The solution was centrifuged to remove cell debris and the resulting supernatant was heated at 60 °C for 10 min to precipitate many of the *E. coli* proteins, which were subsequently removed by centrifugation. The resulting supernatant was subjected to size-exclusion chromatography (SEC: Amersham-Pharmacia, Piscataway, NJ, USA) utilizing a Superose 6 column to isolate intact assembled RGD4C-Fn protein cages. The purified protein cages were characterized by UV-vis spectroscopy, dynamic light scattering (DLS: Brookhaven, 90Plus particle size analyzer), and TEM (LEO 912AB).

Labeling of Ferritin with Fluorescein Dye: Fluorescein-5-maleimide (Molecular Probes, Eugene, OR, USA) was used for fluorescence labeling of ferritin. The dye dissolved in dimethylformamide was mixed with either HFn or RGD4C-Fn in a buffer (100 mM HEPES, 50 mM NaCl, pH 6.5) at the ratio of 3 molar equivalents per ferritin subunit at room temperature for 30 min, followed by overnight incubation at 4 °C. Fluorescein-labeled protein cages were purified with SEC to remove free dye.

Iron Oxide Mineralization inside the Ferritin: Iron oxide mineralization constrained within the HFn and RGD4C-Fn protein-cage structure was performed under an iron-loading factor of 3000 Fe per cage. A degassed solution of 8 mL of 100 mM NaCl and either 1 mg mL^{-1} of HFn (2 mg) or RGD4C-Fn (2.1 mg) in 100 mM NaCl was added to a jacketed reaction vessel under N_2 atmosphere. Ammonium iron(II) sulfate hexahydrate ($(NH_4)_2Fe(SO_4) \cdot 6H_2O$) (12.5 mM, 939 μL) and hydrogen peroxide (H_2O_2, 4.17 mM, 939 μL) were used as an iron source and oxidant, respectively, and were injected into the vessel simultaneously at a constant rate of 31.3 μL min^{-1}. The temperature of the vessel was brought up to and maintained at 65 °C by circulating water through the jacketed flask. The pH was titrated to 8.5 with NaOH (50 mM) (718 Auto Titrator, Brinkmann) during the reaction. The mineralization reaction was considered to be completed 5 min after all the iron and oxidant solutions were injected. Sodium citrate (300 mM, 200 μL) was then added to the mixture, to chelate any free iron. The mineralized RGD4C-Fn was dialyzed into Dulbecco's phosphate buffered saline (DPBS) overnight, followed by purification with SEC to separate from any aggregation products.

FACS Analysis and Epifluorescence Microscopy of Cells Incubated with Fluorescein-Conjugated Ferritin: Human monocyte cell line THP-1 was obtained from the American Type Culture Collection (ATCC). THP-1 cells were cultured in RPMI 1640 (ATTC, 30-2001) supplemented with 10% fetal bovine serum, 2-mercaptoethanol (0.05 mM), penicillin (100 U mL^{-1}), and

streptomycin (100 μg mL^{-1}) at 37 °C in 5% CO_2 atmosphere. For the analysis, the cells suspended in DPBS (with Ca^{2+} and Mg^{2+}) at the concentration of 2.5×10^6 cell mL^{-1} were incubated with fluorescein-conjugated protein cages on ice for 20 min under normalized fluorescein concentration (2 μM). After the incubation, the cells were washed twice with DPBS (with Ca^{2+} and Mg^{2+}) and then resuspended in DPBS (with Ca^{2+} and Mg^{2+}). The fluorescein-conjugated anti-integrin $\alpha_v\beta_3$ mAb (Chemicon MAB1976F) was used as a positive control. Flow cytometry was performed using a FACSCanto (BD Biosciences) and analyzed using FlowJo (Tree Star, Inc.). Epifluorescence microscopy was performed using a Zeiss Axioskop 2 plus microscope. Illumination intensity and camera exposure times were held constant.

Electron Microscopy Study of Cells incubated with the Mineralized Ferritin: Human monocyte-derived macrophages were obtained according to previous work.[23] The cells were incubated with the iron oxide mineralized HFn or RGD4C-Fn for 4 days at concentration of 2 μg mL^{-1} Fn. After 4 days, the cells were washed in PBS twice, followed by rinsing three times in PIPES buffer (100 mM, pH 7.4). Washed cell monolayers were fixed with 4% glutaraldehyde in PIPES buffer for 1 h at 4 °C. Hydrogen peroxide was added to the fixative for a final concentration of 0.3% as a source of oxygen, rendering fixation more efficient. Subsequently, the cells were rinsed three times in PIPES buffer, scraped using a cell scraper, and washed one more time in PIPES buffer. After that, cells were immersed in order of 70, 95, and 100% of ethanol for 5 min. The dehydrated cells were infiltrated under vacuum in LR white resin (Agar Scientific, UK) for 3 days. The LR white was changed every day. The samples were then cured in fresh LR white resin for 23 h at 60 °C. The embedded samples were subsequently sectioned with an ultramicrotome at 40 nm for HAADF-STEM, 70 nm for EFTEM, and 300 nm for 3D electron tomography of HAADF-STEM. All the TEM sections were cut onto 600 mesh, unsupported copper grids. Selected sections were stained with uranyl acetate followed by lead citrate, for 5 min in each solution.

All TEM observations were performed after viewing several hundred cell profiles. Medium-resolution HAADF-STEM study was performed using a Tecnai F20 (FEI; OR, USA) operated at 200 kV using a 30 μm condenser aperture and a camera length of 150 nm. Electron tomography was performed on nonstained 300 nm thick sections. Projections of the object are acquired from several different orientations, and reconstructed into a 3D volume. HAADF-STEM tomographic datasets were acquired over a tilt range of −70° to +70°, using a step size of 2°. 3D reconstruction was carried out using the simultaneous iterative reconstruction technique (SIRT) using Inspect 3D image processing software. Reconstructions were visualized by a voltex projection using Amira™ 3D visualization software (Mercury Computer Systems Inc., Mérignac Cedex, France). EFTEM studies were performed using a CM300 (Philips) operated at 300 kV with a Gatan Imaging Filter (GIF) model 2002, using a 10 μm objective aperture to optimize spatial resolution. To optimize contrast from unstained cells, zero-loss EFTEM images were taken using a 3 eV slit. Iron maps were captured by the three-window technique using Fe $L_{2,3}$ post- and pre-edge.

Cell Viability Assay: Cell viability was assessed using the neutral red assay. Human monocyte-derived macrophages were incubated with the iron oxide mineralized HFn or RGD4C-Fn for 2 days at a concentration of 0–2 μg mL^{-1} Fn. Following incubations, samples were removed and neutral red was added at 40 μg mL^{-1} for 3 h at 37 °C. The cells were rinsed with PBS followed by addition of an extracting solution to dissolve the dye. Absorbance at 570 nm was measured, and cell viability was expressed in % base, where the control sample is set to represent 100% viability. Each experiment was performed in triplicate. Statistics were calculated using a one-way ANOVA, followed by a least-significant difference (LSD) post-hoc test. Significance was taken at $p < 0.01$.

Acknowledgements

This work was funded in part by grants from the National Institutes of Health (R21EB005364) and the Office of Naval Research (19-00-R006 and N00014-03-1-0692). Supporting Information is available online from Wiley InterScience or from the author. This article is part of a Special Issue on Biomaterials.

Received: May 2, 2008
Revised: August 19, 2008
Published online: November 18, 2008

[1] D. F. Emerich, C. G. Thanos, *Biomol. Eng.* **2006**, *23*, 171.
[2] O. C. Farokhzad, R. Langer, *Adv. Drug Deliv. Rev.* **2006**, *58*, 1456.
[3] D. A. Groneberg, M. Giersig, T. Welte, U. Pison, *Curr. Drug Targets* **2006**, *7*, 643.
[4] C. Alric, J. Taleb, G. Le Duc, C. Mandon, C. Billotey, A. Le Meur-Herland, T. Brochard, F. Vocanson, M. Janier, P. Perriat, S. Roux, O. Tillement, *J. Am. Chem. Soc.* **2008**, *130*, 5908.
[5] J. Kim, J. E. Lee, S. H. Lee, J. H. Yu, J. H. Lee, T. G. Park, T. Hyeon, *Adv. Mater.* **2008**, *20*, 478.
[6] H. Park, J. Yang, S. Seo, K. Kim, J. Suh, D. Kim, S. Haam, K. H. Yoo, *Small* **2008**, *4*, 192.
[7] M. Uchida, M. L. Flenniken, M. Allen, D. A. Willits, B. E. Crowley, S. Brumfield, A. F. Willis, L. Jackiw, M. Jutila, M. J. Young, T. Douglas, *J. Am. Chem. Soc.* **2006**, *128*, 16626.
[8] M. L. Flenniken, D. A. Willits, A. L. Harmsen, L. O. Liepold, A. G. Harmsen, M. J. Young, T. Douglas, *Chem. Biol.* **2006**, *13*, 161.
[9] P. A. Suci, Z. Varpness, E. Gillitzer, T. Douglas, M. Young, *Langmuir* **2007**, *23*, 12280.
[10] P. Couvreur, C. Vauthier, *Pharm. Res.* **2006**, *23*, 1417.
[11] T. Douglas, M. Young, *Science* **2006**, *312*, 873.
[12] M. Manchester, P. Singh, *Adv. Drug Deliv. Rev.* **2006**, *58*, 1505.
[13] M. Uchida, M. T. Klem, M. Allen, M. L. Flenniken, E. Gillitzer, Z. Varpness, P. Suci, M. J. Young, T. Douglas, *Adv. Mater.* **2007**, *19*, 1025.
[14] M. L. Flenniken, D. A. Willits, S. Brumfield, M. Young, T. Douglas, *Nano Lett.* **2003**, *3*, 1573.
[15] M. Uchida, M. Terashima, C. H. Cunningham, Y. Suzuki, D. A. Willits, A. F. Willis, P. Yang, P. Tsao, M. V. McConnell, M. J. Young, T. Douglas, *Magn. Reson. Med.* **2008**, *60*, 1073.
[16] W. Arap, R. Pasqualini, E. Ruoslahti, *Science* **1998**, *279*, 377.
[17] E. Ruoslahti, T. Duza, L. Zhang, *Curr. Pharm. Design* **2005**, *11*, 3655.
[18] T. V. Byzova, R. Rabbani, S. E. D'Souza, E. F. Plow, *Thromb. Haemost.* **1998**, *80*, 726.
[19] A. S. Antonov, F. D. Kolodgie, D. H. Munn, R. G. Gerrity, *Am. J. Pathol.* **2004**, *165*, 247.
[20] S. Tsuchiya, Y. Kobayashi, Y. Goto, H. Okumura, S. Nakae, T. Konno, K. Tada, *Cancer Res.* **1982**, *42*, 1530.
[21] S. Benedetto, R. Pulito, S. G. Crich, G. Tarone, S. Aime, L. Silengo, J. Hamm, *Magn. Reson. Med.* **2006**, *56*, 711.
[22] A. E. Porter, M. Gass, K. Muller, J. N. Skepper, P. Midgley, M. Welland, *Environ. Sci. Technol.* **2007**, *41*, 3012.
[23] A. E. Porter, K. Muller, J. Skepper, P. Midgley, M. Welland, *Acta Biomater.* **2006**, *2*, 409.
[24] A. E. Porter, M. Gass, K. Muller, J. N. Skepper, P. A. Midgley, M. Welland, *Nat. Nanotechnol.* **2007**, *2*, 713.
[25] A. Vonarbourg, C. Passirani, P. Saulnier, J. P. Benoit, *Biomaterials* **2006**, *27*, 4356.
[26] K. Muller, J. N. Skepper, M. Posfai, R. Trivedi, S. Howarth, C. Corot, E. Lancelot, P. W. Thompson, A. P. Brown, J. H. Gillard, *Biomaterials* **2007**, *28*, 1629.
[27] M. E. Kooi, V. C. Cappendijk, K. Cleutjens, A. G. H. Kessels, P. Kitslaar, M. Borgers, P. M. Frederik, M. Daemen, J. M. A. van Engelshoven, *Circulation* **2003**, *107*, 2453.
[28] A. G. Dupuy, E. Caron, *J. Cell Sci.* **2008**, *121*, 1773.
[29] J. Savill, I. Dransfield, N. Hogg, C. Haslett, *Nature* **1990**, *343*, 170.
[30] R. Hanayama, M. Tanaka, K. Miwa, A. Shinohara, A. Iwamatsu, S. Nagata, *Nature* **2002**, *417*, 182.